World Academy of Science, Engineering and Technology
International Journal of Electrical and Computer Engineering
Vol:17, No:5, 2023

# Optimal Efficiency Control of Pulse Width Modulation - Inverter Fed Motor Pump Drive Using Neural Network

O. S. Ebrahim, M. A. Badr, A. S. Elgendy, K. O. Shawky, P. K. Jain



***Abstract*****—**This paper demonstrates an improved Loss Model Control (LMC) for a 3-phase induction motor (IM) driving pump load. Compared with other power loss reduction algorithms for IM, the presented one has the advantages of fast and smooth flux adaptation, high accuracy, and versatile implementation. The performance of LMC depends mainly on the accuracy of modeling the motor drive and losses. A loss-model for IM drive that considers the surplus power loss caused by inverter voltage harmonics using closed-form equations and also includes the magnetic saturation has been developed. Further, an Artificial Neural Network (ANN) controller is synthesized and trained offline to determine the optimal flux level that achieves maximum drive efficiency. The drive's voltage and speed control loops are connecting via the stator frequency to avoid the possibility of excessive magnetization. Besides, the resistance change due to temperature is considered by a first-order thermal model. The obtained thermal information enhances motor protection and control. These together have the potential of making the proposed algorithm reliable. Simulation and experimental studies are performed on 5.5 kW test motor using the proposed control method. The test results are provided and compared with the fixed flux operation to validate the effectiveness.

***Keywords*****—**Artificial neural network, ANN, efficiency optimization, induction motor, IM, Pulse Width Modulated, PWM, harmonic losses.

## NOMENCLATURE

| | |
|---|---|
| $I_s$, $I_r'$ | Stator, rotor referred current |
| $I_m$ | Magnetizing current |
| $I_i$ | Iron-loss equivalent current |
| $V_s$ | Stator voltage |
| $E$ | Air gap voltage |
| $R_s$, $R_r$ | Stator, rotor winding resistance |
| $X_s$, $X_r$ | Stator, rotor self reactance |
| $X_m$ | Magnetizing reactance |
| $\sigma$ | Leakage factor [$\sigma = 1\text{-}X_m^2/X_sX_r$] |
| $R_r'$ | Referred rotor resistance [$R_r' = (X_s/X_m)^2R_r$] |
| $X_r'$ | Referred rotor reactance [$X_r' = \sigma X_s/(1\text{-}\sigma)$] |
| $s$ | Slip |
| $a$,$\omega$ | Stator frequency |
| $\omega_r$ | Rotor electrical speed |
| $\omega_b$ | Base frequency |
| $\psi_s$ | Stator flux linkage |
| $T_e$ | Electromagnetic torque |
| $T_L$ | Load torque |
| $C_e$, $C_h$ | Eddy, hysteresis loss coefficient |
| $C_{str}$, $C_{fw}$ | Stray, mechanical loss coefficient |
| $C_{mi}$ | The $i^{th}$ coefficient of magnetizing curve |
| $C_{con1}$, $C_{con2}$ | Converter losses coefficients |

## I. INTRODUCTION

RAPID escalation in both energy prices and environmental pollution awareness has significant impacts on the community. Therefore, it becomes imperative that major attention be paid to improve system efficiency. Fluid pumping is perhaps the most common process in industrial plants and household applications. A substantial amount of energy can be saved by using variable-speed electric motor drive (VSD) to control fluid flow instead of mechanical throttling valves or bypassing. Besides, the VSD prevents catastrophic surge pressure (known as fluid hammer) that causes severe mechanical stress in the pipe system, or even damage, by offering smooth start/stop pumping [1].

IMs have the advantages of high reliability, ruggedness, and low cost of machine manufacturing. On the other hand, advances in power switching devices and digital signal processors have significantly matured the voltage-source inverters (VSIs) with associated pulse width modulation (PWM) techniques. As a result, PWM-VSI fed IM has been well established as the foremost structure for the ac VSD systems. Using hard switched integrated-gate bipolar transistor (IGBT) or integrated-gate commutated thyristor (IGCT) modules working at moderate switching frequency (1-2 kHz), in conjunction with a pulse filter for overvoltage spikes and bearing currents mitigation in case of long cable length, is the common industry practice to provide economical motor pump drive. This is because most soft-switching techniques, to realize high switching frequency and hence compact sinusoidal output filter, require extra switching components and hence; increased cost [2], [3].

Power losses in the IM drive are greatly dependent on the control strategy. Fast torque response is not a crucial requirement in the pumping applications. Therefore, IM drives in such plants are usually based on the scalar V/f control method as illustrated schematically in Fig. 1 (a). In this method, the ratio

O. S. Ebrahim, Dr., is with the Dept. of Electrical Power and Machines, Ain-Shams University, Egypt (e-mail: osama.shawky@eng.asu.edu.eg).
M. A. Badr is Prof. and Vice President of the Future University, Egypt (e-mail: mabadr@fue.edu.eg).
A. S. Elgendy is Eng. (e-mail: engalisabry@yahoo.com).
K. O. Shawky, Student, is with the Civil Dept., Ain-Shams University, Egypt (e-mail: kareem.osama@eng.asu.edu.eg).
P. K. Jain, Prof. and Director of ePOWER Research Center, Queen's University, Canada (e-mail: praveen.jain@queensu.ca).

of the stator voltage to frequency and hence machine flux is maintained constant as long as the speed is below rated. The method does satisfy pump's application requirements, while keeping the flux constant deteriorates motor efficiency, in particular at low speeds with partial load.

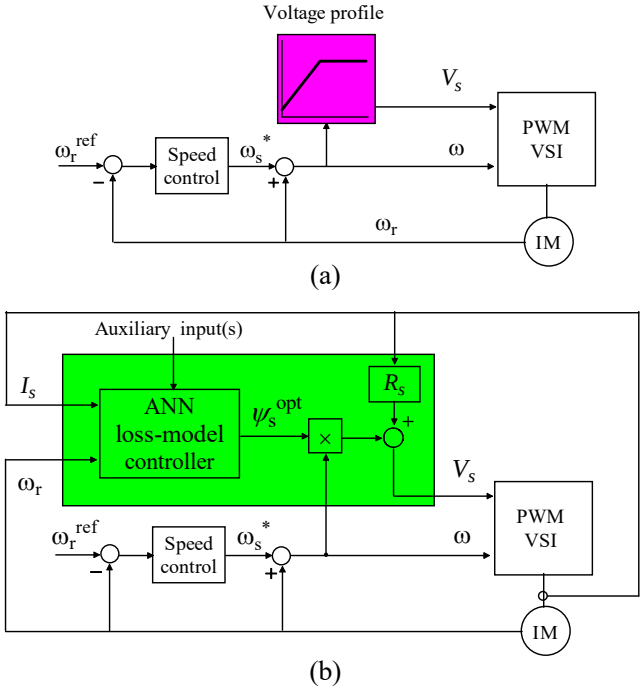


Fig. 1 (a) Classical V/f control and (b) proposed control

In an effort to improve the IM efficiency, various flux control methods have been developed. These methods can be broadly classified into two groups: search control (SC) and loss model control (LMC). The basic principle of SC is to measure the input power and then iteratively search for the flux level (or its equivalent variables) until the minimum input power is detected for a given torque and speed [4], [5]. Major drawbacks of SC are: slow convergence rate, flux/ torque ripples, difficulties in tuning the algorithm for a given application, and the need for precise measurement of the input power which is difficult and costly. On the other hand, the LMC computes the optimum flux level that minimizes losses through a machine model [6]-[13]. LMC approach provides smooth and fast adaptation of the machine flux with low implementation cost. However, LMC requires correct modeling of the motor drive and the losses.

Application of LMC to the vector [6]-[9] and scalar [10]-[12], controlled IM drives has been proposed using different steady state models and implementation techniques. When the model disregards the core loss and magnetic saturation, the optimal stator flux (i.e., the flux where the efficiency is maximum) is uniquely determined by the speed [13]. The idea of searching for maximum efficiency by use of a LMC including the core loss and magnetic saturation has also been addressed. In this case, the optimal flux (or slip) varies not only with the speed, but also with the load torque [10]. The load torque is replaced by the stator current in [11] and [12] to remove the necessity of load torque measurement or estimation. However, two problems need to be solved to make this method viable. One is that the excess iron loss under PWM voltage supply plays a rule in estimating the motor efficiency and therefore it should be included in the loss model [14]. However, representation of this loss component by measurements [15], [16] yields discrepancies between the results due to the absence of a governing law with valid assumptions. The second problem is that the algorithm is most likely implemented using a lookup table which has limited performance in terms of size with the required accuracy especially; in case of multi-inputs.

In [17], the authors introduced a novel LMC system for the scalar IM drives. Fig. 1 (b) demonstrates a generic layout of this system. An ANN controller is trained offline to generate the optimal stator flux value that maximizes the drive's efficiency using a more detailed loss model. The model includes the surplus power iron and copper losses in PWM regime using closed form equations and taking the magnetic circuit saturation into account. A gradient-descent algorithm is designed to solve the optimization problem and provides behavioral examples to learn the ANN controller. The ANN can provide accurate function approximation with custom design at low cost where it is possible to accommodate, for example, the drive's thermal model in a straightforward way by including temperature as an auxiliary input. The amounts of power saved in the IM vary with the load type. The load information is represented by the rotor speed and stator current signals. The flux control is selected here since it is more suitable for the pump plants where the load torque is proportional to the square of the speed. It also takes advantage of low speed. Furthermore, linking the flux and speed control loops to generate the stator voltage reference from the ANN output and stator frequency command avoids the possibility of excessive magnetization during transient periods.

This paper demonstrates how model parameters variations due to temperature changes can be accommodated in the ANN controller using biasing source. A first-order thermal model is developed such that the monitored thermal information can be utilized to improve the performance of motor's control and protection system as well. These have the potential of making the proposed algorithm comparatively reliable. To verify the concept, the performance is tested in both simulation and experimentation and the results show enhancement in terms of power savings.

In the following, this loss minimization method in IM drives is introduced. In Section II, the relationships between the IM variables considering an equivalent circuit in the stator flux reference frame are given. In Section III, the proposed loss model is presented. In Section IV, a gradient descent search algorithm has been designed to minimize power loss and the problems related to algorithm implementation are discussed. To alleviate these problems, the ANN control concept is proposed as in Section V. Simulation and experimental results using 5.5 kW variable speed pump are presented in Section VI. The conclusions are addressed in Section VII.

## II. IM Equivalent Circuit

The equivalent circuit for IM can be varied by the different

choices of flux linkage constants. In this work, we utilize an equivalent circuit referenced to the stator magnetizing current by defining the stator flux linkage as $\psi_s = X_s I_m$. Fig. 2 illustrates the notation of this transformation at steady state. The selected circuit configuration avoids leakage reactance separation error and is adequate for stator flux control. The saturation of the main flux path is modeled by a nonlinear inductor $X_s(\psi_s)$ while iron loss variation due to operating frequency change is represented by a nonlinear resistor $R_i(a,s)$. The saturation of leakage flux path affects machine transient performance during the starting and braking modes. However, it can be neglected during normal operation without noticeable errors [11], [18]. The circuit parameters are derived from no-load and blocked rotor tests using pure sinusoidal supply and represented in per unit system. The per unit stator frequency is related to $\omega_r$ by

$$a = \frac{\omega}{\omega_{base}} = \frac{\omega_r}{1-s}\ . \tag{1}$$

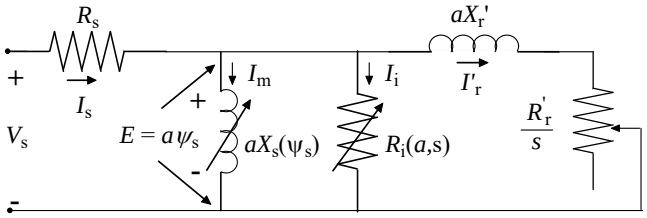


Fig. 2 An IM equivalent circuit

From Fig. 2, the stator current is given by

$$I_s = \sqrt{(I_m + I'_r \sin\phi_r)^2 + (I_i + I'_r \cos\varphi_r)^2}\ , \tag{2}$$

where

$$\tan\phi_r = \frac{aX'_r}{(R'_r/s)}.$$

The magnetizing current is

$$I_m = \frac{E}{aX_s(\psi_s)} = \frac{\psi_s}{X_s(\psi_s)} \tag{3}$$

Equation (3) can be rewritten as a series of order *k* in order to include magnetic saturation

$$I_m(\psi_s) = \sum_{i=0}^{k} C_{mi}(\psi_s)^i\ . \tag{4}$$

The iron-loss equivalent current is calculated from

$$I_i = \frac{E}{R_i(a,s)}, \tag{5}$$

where $R_i(a,s) = [C_e(1+s^2) + C_h(1+s)/a]$.

The rotor current can be determined in terms of stator flux as

$$I'_r = \frac{\psi_s}{\sqrt{(R'_r/as)^2 + X'^2_r}}. \tag{6}$$

The electromagnetic torque is given by

$$T_e = I'^2_r \frac{R'_r}{as}. \tag{7}$$

Substitution from (6) into (7) yields

$$T_e = \psi_s^2 \frac{(R'_r/as)}{(R'_r/as)^2 + X'^2_r}. \tag{8}$$

## III. Proposed Loss Model

### A. Fundamental IM Losses

With a sinusoidal supply voltage amplitude equal to the fundamental inverter voltage; the IM's loss-components are:

Iron losses:

$$P_i = [C_e(1+s^2)a^2 + C_h(1+s)a]\psi_s^2\ . \tag{9}$$

Copper losses:

$$P_{cu} = R_s I_s^{\ 2} + R'_r I'^2_r\ . \tag{10}$$

Friction and windage losses:

$$P_{fw} = C_{fw}\omega_r^2\ . \tag{11}$$

Stray losses:

$$P_{str} = C_{str}\omega_r^2 I'^2_r\ . \tag{12}$$

The expression of the stray losses holds for dc motor and also acceptable for IM [4].

### B. PWM Harmonic Loss

The PWM inverter generates voltage harmonics which cause excess iron and copper losses in the machine. Hence, one can expect errors in the performance of a LMC designed based on the fundamental losses only. To alleviate this problem, the PWM harmonic loss is included here using closed-form expressions. In the following, a sinusoidal PWM inverter is assumed to be feeding the machine.

1. PWM Harmonic Iron Loss

Following [19], the governing equation of the surplus eddy loss due to PWM voltage harmonics can be deduced as

$$P_{eddy}^{PWM} = (F_c^2 - 1)P_{eddy}\ . \tag{13}$$

where, $P_{eddy} = C_e(1+s^2)a^2\psi_s^2$ is the classical eddy loss under pure sinusoidal regime. The PWM form factor $F_c$ is defined as the ratio of PWM to sinusoidal form factors. For an inverter operating in the linear region of sinusoidal modulation, $F_c$ can be calculated in terms of voltage modulation index $m$ as

$$F_c = \frac{1.15}{\sqrt{m}}, \qquad m \le 1. \tag{14}$$

With a constant dc-link voltage $V_{dc}$ and frequency modulation ratio ≥ 20, the fundamental inverter output voltage (i.e., fundamental stator voltage) is given by

$$V_s = 0.612\frac{m}{V_{dc}}. \tag{15}$$

Ignoring the stator resistive drop, (15) can be approximated as

$$m = 1.63\frac{a\psi_s}{V_{dc}}. \tag{16}$$

It is worth mentioning that the nonlinear region of the inverter operation is rich by undesirable harmonics and therefore; it is replaced by square-wave mode in practical drives. Further, the IM energy control is effective especially when the motor operates at low speed under a light load. In such a case, minimization of the motor losses implies reduction in the stator flux level and hence stator voltage below rated. Thus, restriction of (14) to the linear region of inverter operation does not represent a performance limit.

If the stator resistive drop is neglected, the relation between the value of PWM peak stator flux and its first harmonic peak value is near unity. Since the hysteresis loss is proportional to the flux peak, its variation under sinusoidal and PWM regimes is negligible [19].

2. PWM Harmonic Copper Loss

Here, neglecting the skin effect is a reasonable assumption by considering: (i) the stator conductors interleaving or transposition and (ii) magnetic bridging of semi-closed rotor slot structure which is a common design for inverter-fed cage IM [20]-[22].

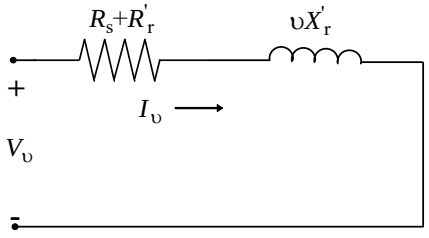


Fig. 3 An Equivalent circuit at the υ[th] harmonic frequency

The PWM inverter produces voltage harmonics at the switching frequency $f_s$. Fig. 3 shows IM equivalent circuit at a harmonic order υ = $f_s$ with the harmonic slip ($s_\upsilon$ = 1–$\omega_r$ / $f_s$) approximated to unity. The PWM harmonic copper loss is

$$P_{cu}^{PWM} = I_\upsilon^2(R_s + R_r'). \tag{17}$$

Since $f_s X_r' >> (R_s + R_r')$, the switching harmonic current $I_\upsilon$ is given by

$$I_\upsilon = \frac{V_\upsilon}{f_s X_r'}. \tag{18}$$

For a sinusoidal PWM inverter, the switching harmonic voltage $V_\upsilon$ can be determined in terms of the harmonic distortion function $HDF_{SPWM}$ as [23]

$$V_\upsilon = V_{dc}\sqrt{\frac{HDF_{SPWM}}{48}}. \tag{19}$$

where

$$HDF_{SPWM} = \frac{3}{2}m^2 - \frac{4\sqrt{3}}{\pi}m^3 + \frac{9}{8}m^4. \tag{20}$$

*C. Proposed Loss Model*

The total loss $P_{loss}$ is obtained by adding the fundamental and PWM-harmonic losses. From the analysis given in Sections II and III, it can be shown that

$$\left.\begin{aligned} P_{loss} &= P_i + P_{cu} + P_{fw} + P_{str} + P_{eddy}^{PWM} + P_{cu}^{PWM} + P_{con} \\ &= \Phi(a, \psi_s, \omega_r) \end{aligned}\right\} \tag{21}$$

The converter loss $P_{con}$ is presented in (21) in order to account for power losses in the rectifier and inverter circuits of the drive. It can be approximated by

$$P_{con} = C_{con1}I_s + C_{con2}I_s^2. \tag{22}$$

Equation (21) is a flux dependent function with a minimal point. Thus, there is an optimal value for the stator flux that minimizes power losses and at the same time satisfies load requirements. Due to complexity, solving this total loss minimization based problem is feasible using numerical methods.

## IV. Optimization Algorithm

A gradient-descent optimization algorithm is designed in order to find the optimal stator flux value that minimizes (21) at a given rotor speed and load torque. Fig. 4 demonstrates the algorithm flowchart. The concept of the algorithm is to vary $\psi_s$ as a function of the power consumption until the point of minimum losses, which simultaneously fulfils the loading condition, is found. To facilitate IM circuit analysis, the program takes motor slip as the independent variable and starts

by assuming an initial value $s_o$ for the specified load torque $T_L$ and rotor speed $\omega_r$. The pu stator frequency $a$ and the electromagnetic torque $T_e$ at rated flux are then calculated from (1) and (10), respectively. The value of $\psi_s$ to produce $T_L$ is evaluated, utilizing the quadratic proportionality between torque and flux, to be used in the loss function $\Phi(a, \psi_s, \omega_r)$ calculation. The search loop terminates if the change $\Delta\Phi$ is less than an arbitrary small value $\varepsilon$. Otherwise, it resumes by changing the slip in the direction of negative gradient, that is determined by $-\text{sign}(\Delta\Phi)$ where $\text{sign}(\Delta\Phi) = 1$ if $\Delta\Phi > 0$ and $\text{sign}(\Delta\Phi) = -1$ if $\Delta\Phi < 0$, by a constant step size $h$ till the point of minimum losses is obtained [24]. To make sure that the algorithm is not trapped in a local minimum, the search loop is executed at each loading point more than once starting from different initial slip values.

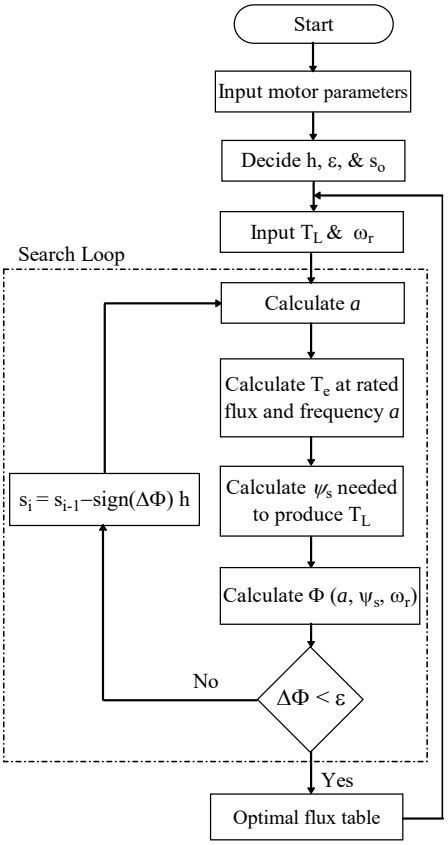


Fig. 4 Flowchart of gradient-descent optimization algorithm

A review of the relevant literature shows that LMC has been implemented using two approaches. The first approach is to sectionalize the loss model calculations and run the algorithm, as a background process on the Digital Signal Process (DSP), at a slower sampling rate than the speed control loop [12]. When this principle is used, it is also possible to adapt model parameters through online identification. However, a proper updating rate of the reference flux depends on the DSP computational power and the dynamics of the outer process operated by the drive. Another way of implementation is to do all the LMC calculations offline and store the results in a two-dimensional lookup table, so that during operation the drive will be controlled according to this table [10], [11]. This solution is simple with little demand on the DSP. But, the lookup table, as realized by storing digital words on the DSP memory, has limited performance in terms of size with the required accuracy.

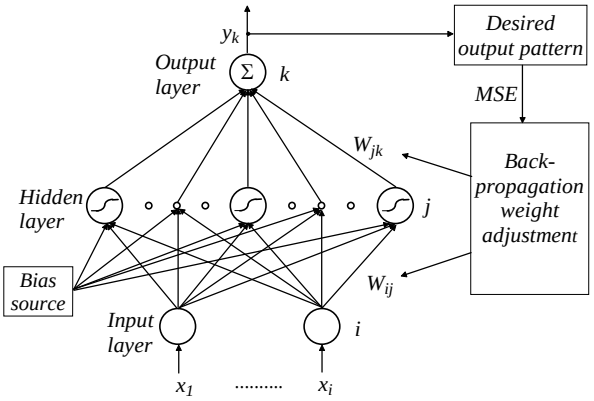


Fig. 5 Three-layer feedforward ANN

## V. ANN Flux Controller

The ANN is selected here to realize the optimal energy control algorithm. Using the ANN instead of a lookup table has the advantages of parallel processing, noise reduction, and high accuracy/cost ratio [25], [26]. Further, the ANN design is flexible and can accommodate extra input or model parameter variations in a systematic way by employing additional input indicators (biasing sources), for example the temperature, without adding greatly to the resources (see Appendix A).

Fig. 5 shows configuration of a three-layer feedforward network having input and output layer neurons dictated by the number of respective signals and hidden layer neurons with sigmoid transfer functions. This configuration is able to approximate any function with a finite number of discontinuities after training using set of examples for the network behavior [27]. The training data are obtained from the mathematical model of the drive and executing the optimization algorithm offline. The data comprise load information as an input pattern and the corresponding optimal stator flux as an output pattern. To avoid load torque measurement or estimation, the load torque can be replaced by the stator current signal which is usually accessible in the drive systems for protection purposes. For a pump load with constant head, the quadratic relationship between the speed and torque is unique [28]. In such a case, the rotor speed signal contains sufficient information to withstand as the only load indicator.

Once the example data are prepared and the weights and biases are initialized, the network is ready for learning. We consider that the network is being trained by the input pattern $n$, the weights and biases of the network are adjusted using the back-propagation technique to minimize the network performance function. A common performance function for the feedforward networks is the mean squared error (MSE):

$$MSE = \frac{1}{Q}\sum_{k=1}^{Q}(d_k^n - y_k^n). \quad (23)$$

where $d_k^n$ = desired output of the kth neuron in the output layer, $y_k^n$ corresponding actual output, and $Q$ = dimension of the output vector (in our case $Q$ = 1). The weights of the neurons are altered to minimize the value of MSE by gradient descent method. The weight update equation is then given as

$$W_{ij}(l+1) = W_{ij}(l) - \eta \frac{\partial MSE}{\partial W_{ij}(l)}. \quad (24)$$

where $\eta$ = learning rate, $W_{ij}(l+1)$ = new weight between $i^{th}$ and $j^{th}$ neurons, and $W_{ij}(l)$ corresponding old weight. The weights are iteratively updated for all the $N$ training patterns. A momentum term $\mu[W_{ij}(l+1) - W_{ij}(l)]$ is usually added to the right hand side of (24), where is $\mu$ is a small value, in order to improve training performance.

Running the LMC with a voltage control loop independent of the speed control loop is not recommended in practice because there is a possibility for the machine to operate under heavy saturation, even with a stator voltage below rated, due to discrepancy between the actual and calculated stator frequencies caused by the modeling errors. Therefore, the ANN output is selected here to be the optimal stator flux instead of stator voltage. This has the potential for making the drive comparatively reliable since the voltage and speed control loops are linked by the actual stator frequency as demonstrated in Fig. 1 (b).

The stator voltage magnitude is approximated by

$$V_s = \omega\psi_s + R_s I_s. \quad (25)$$

The above approximation has no noticeable effect on the efficiency control, particularly, in case of pump systems where the input current is proportional to the speed [29].

## VI. Simulation and Experimental Results

To verify the validity and effectiveness of the proposed control scheme, simulation and experimental studies have been carried out. The simulation and experimental results, shown in Figs. 6-17, are obtained with a 3-phase IM fed from a sinusoidal PWM inverter and loaded by a centrifugal water pump having constant head of 15 m. The 5.5 kW, 380 V, 50 Hz, 2-pole, delta-connected, IM parameters are $R_s$ = 0.0338, $R_r'$ = 0.051, $X_r'$ = 0.049, $C_e$ = 0.06, $C_h$ = 0.035, $C_{str}$ = 0.01 whilst the inverter specifications are: $f_s$ = 20, $V_{dc}$ = 1.59, $C_{con1}$ = 0.01, $C_{conv2}$ = 0.001. The IM parameters and inverter specifications are expressed in a per unit system of 5.5 kW base power, 380 V base voltage, and 314 rad/s base angular frequency. The measured magnetizing current as a function of the stator flux is given in Fig. 6 while the measured pump torque-speed curve at the specified head is shown in Fig. 7.

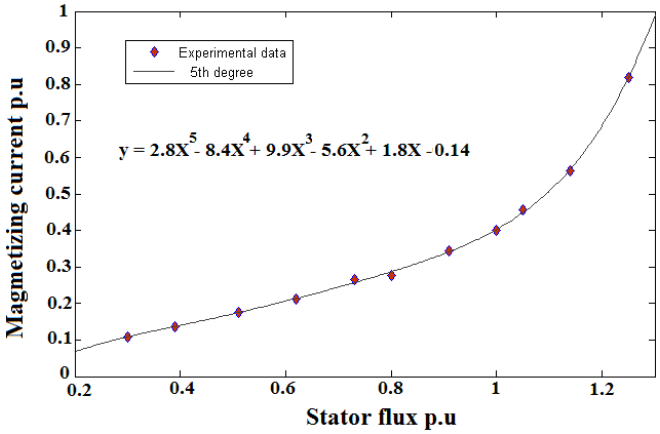


Fig. 6 Measured data of the magnetizing current

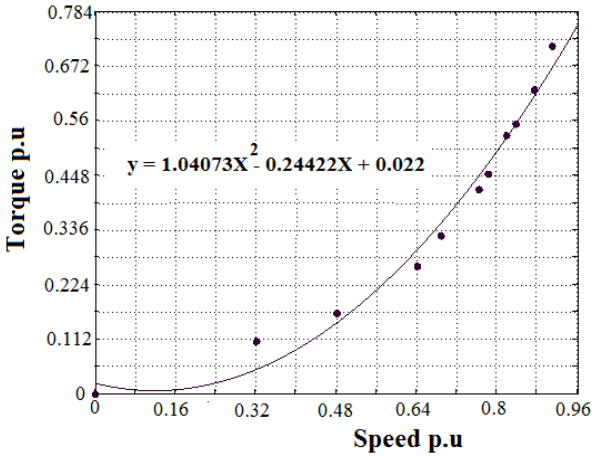


Fig. 7 Measured pump torque-speed curve

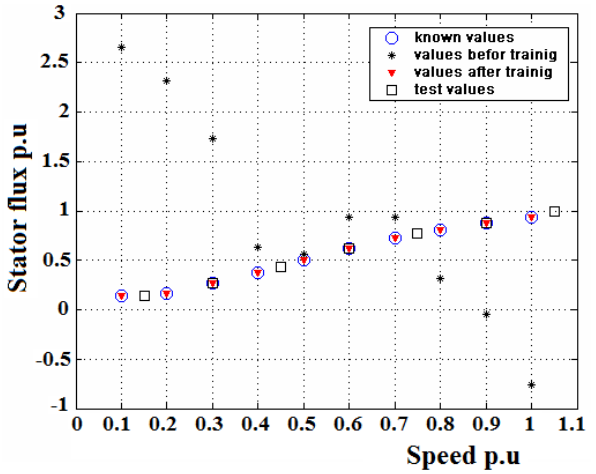


Fig. 8 ANN testing

The gradient-descent optimization algorithm is executed on MATLAB platform and the results are used to train the ANN controller [27]. Since the pump head is constant, the quadratic relation between the pump torque and speed is unique. Therefore, it was sufficient to train the ANN and represent results considering the speed as the only load indicator. The

ANN configuration is chosen as follows: input layer, output layer, and hidden layer with activation function = tan-sigmoid. Fig. 8 shows the desired stator flux and ANN output before and after network learning with $\eta = 0.7$, $\mu = 0.1$, and $N = 10$. The calculated network performance measure, MSE, is approaching $10^{-10}$. The figure also illustrates the ANN output at some test points where it can be concluded that the selected ANN structure emulates gradient-descent optimization algorithm precisely enough for an accurate control.

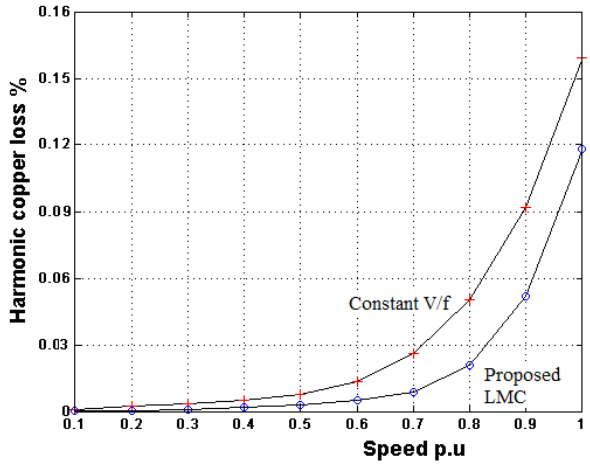


Fig. 9 PWM harmonic copper loss

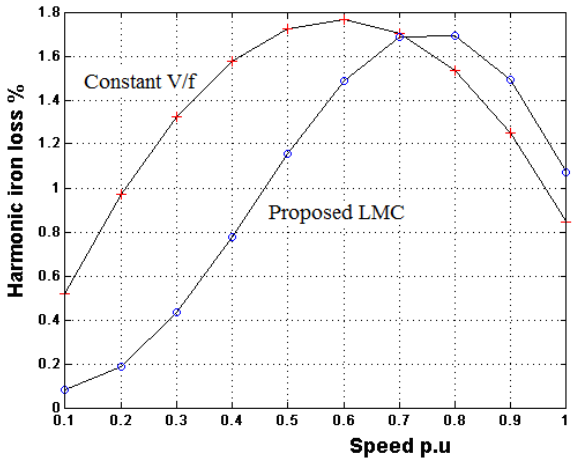


Fig. 10 PWM harmonic iron loss

The whole drive system is simulated and the performance of proposed LMC is compared with that obtained by the classical V/f control. The results of comparison are shown in Figs. 9-13 at steady state. Figs. 9 and 10 show the harmonic copper and iron losses, respectively, in terms of the rotor speed. It can be noted that the harmonic iron loss is much higher than the harmonic copper loss and constitutes a noticeable amount of the total losses that is shown in Fig. 11. From (17) and (18) it follows that the harmonic copper loss is inversely proportional to the switching frequency square. Therefore, its contribution can be neglected without significant errors in the case of small power drives where high switching frequency is not problematic. The objective of the energy control is to minimize the total loss function, not an individual loss component. As anticipated, Fig. 11 depicts that this objective is realized despite the relative increase in PWM iron loss with flux control that is shown in Fig. 10 at $\omega_r \geq 0.7$ p.u is owing to collapsed behavior of (13) with the stator voltage. Figs. 12 and 13 demonstrate the reduction in the stator current and improvement in drive efficiency, respectively, as a result of application of the proposed control.

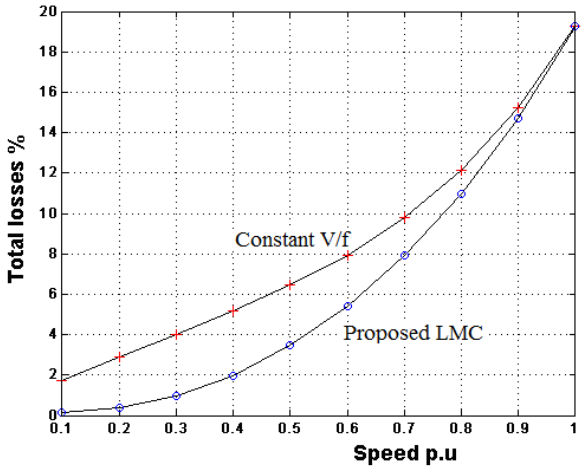


Fig. 11 Total power loss

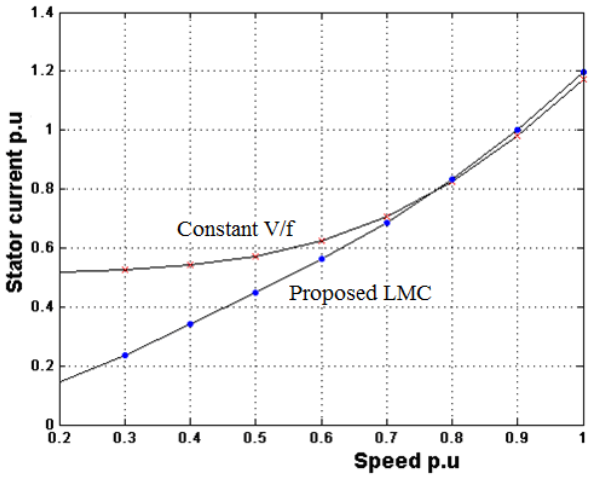


Fig. 12 Stator current

Fig. 14 illustrates the influence of IM modeling on the amount of power saving that can be achieved by a programmed flux control rather than constant flux control. Three IM modeling strategies are studied and compared. The first and simplest one assumes a linear equivalent circuit for the IM and considers the inverter as an ideal controllable voltage source. The second modeling approach takes the magnetic saturation effect into account, while the last scheme, proposed here, includes PWM harmonic losses as well. In each case, the optimal flux value is determined based on the assumed IM equivalent circuit and corresponding loss-model while the actual power loss is calculated by substituting these flux values into (21). From Fig. 14 it is evident that the proposed modeling

strategy increases the percentage of power saving, particularly at low speeds.

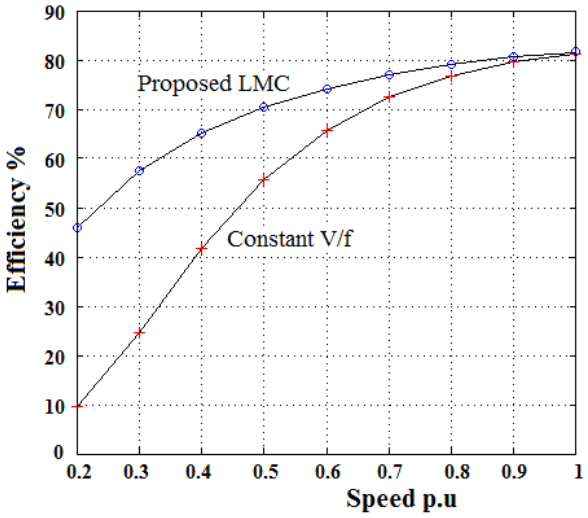


Fig. 13 Drive efficiency

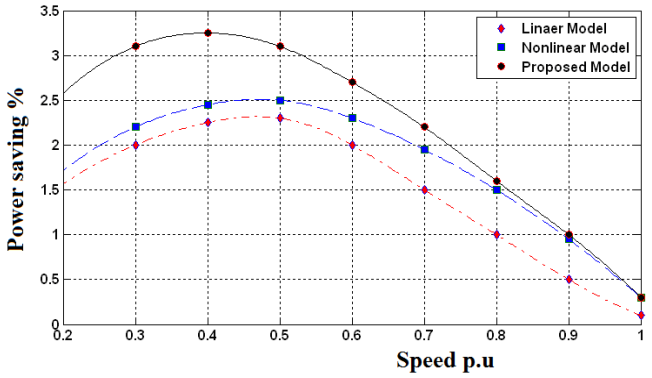


Fig. 14 Power saving of different modeling strategies

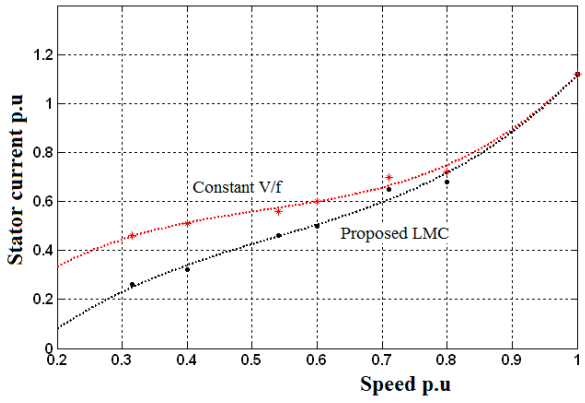


Fig. 15 Measured stator current

Analysis showed that, for a totally enclosed fan cooled (TEFC) motor driving pump, the errors due to resistance changes with temperature are substantial during initial cold motor state. Whereas; it can be neglected after a running time greater than the thermal time constant by considering hot resistance values in the LMC. This is because, in case of TEFC motor driving pump, both the motor heating and fan cooling are proportional to the shaft speed square. Hence the steady state temperature is nearly constant at its operational value irrespective of the speed.

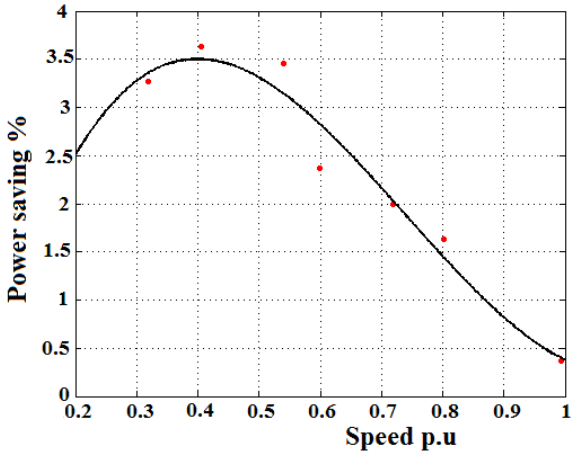


Fig. 16 Measured power saving using proposed control

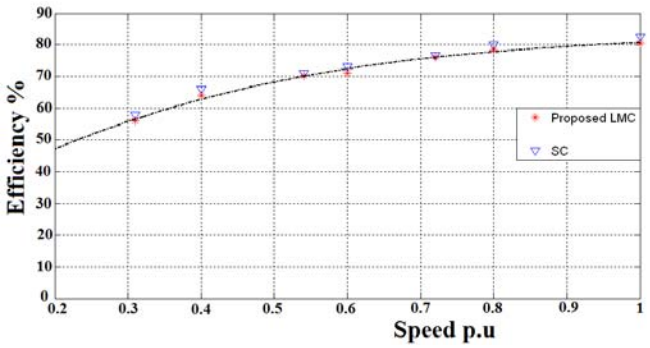


Fig. 17 Measured drive efficiency using SC and the proposed LMC

For further investigation of the proposed LMC, experimental tests are performed. The ANN output at specified rotor speeds is used to calculate the stator voltage reference, as in (25), and the results are programmed on an EEPROM module to adjust the voltage profile of the inverter in accordance [30]. Figs. 15 and 16 show the measured motor current and percentage of power saving, respectively, compared with the classical V/f control. Fig. 17 shows the drive efficiency in comparison with that obtained using SC. The results agree with the corresponding simulations and validate the method.

## VII. Conclusion

This paper has presented an improved LMC algorithm for the scalar IM drives. The method utilizes a loss-model that can give more insight physical-view and accurate results by considering the PWM harmonic losses and magnetic saturation using closed form equations. It was shown through simulation and experimentation that these effects have an impact on the optimal flux value and thus on the amount of energy saving. The implementation of the introduced scheme is made viable for industrial fields by applying the ANN control concept. The

ANN controller offers accurate performance and customization of design at low cost. Handling the effect of temperature variation through first-order thermal model enhances motor protection and control. The proposed algorithm can be extended for sensorless IM pump drive utilizing open/closed loop speed estimator [32].

## ACKNOWLEDGMENT

We are sincerely grateful to Prof. M. A. Hellal, Mechanical and Electrical Research Institute (MERI), National Water Research Center, Egypt and the people who helped us during writing phase of this work. The authors are also thankful to the reviewers for their useful suggestions to revise the paper.

## APPENDIX A

Basically, motor thermal modeling for digital protection and control depends on the $I^2t$ principle and is derived from the first-order thermal model in (26) [3], [31]:

$$\frac{d\theta}{dt} = \frac{1}{\tau}(\theta_f - \theta) \tag{26}$$

where $\theta, \theta_f,$ and $\tau$, respectively, are temperature-rise (above ambient), final temperature-rise (above ambient), and thermal time constant. The recursive temperature solution to (26) is given in (27):

$$\theta_n = \theta_{n-1} + (\theta_f - \theta_{n-1})(1 - e^{-\frac{\Delta t}{\tau}}) \tag{27}$$

where $\theta_n$, $\theta_{n-1}$, and $\Delta t$ , respectively, are the calculated present temperature, temperature at previous time step and time step between calculations. Further, $\theta_f = (I/I_{ref})^2 T_{ref}$ where *I, $I_{ref}$,* and $T_{ref}$, respectively, are the motor phase current, set current reference, and set temperature rise reference. Thermal Capacity Used (TCU) is calculated based on rated motor current with an overload factor applied and expressed as a percentage of maximum temperature. The thermal protection trips when TCU reaches 100%.

The variation of the stator and rotor resistances with temperature is assumed to follow the relation [20]:

$$R(\theta_n) = R(\theta_{n-1}) + \alpha\Delta\theta \tag{28}$$

where, α is the temperature coefficient of resistance for the conductor's martial.

## REFERENCES

[1] US Department of Energy, Lawrence Berkeley National Laboratory, "Variable speed pumping: A guide to successful applications," 2004.

[2] Y. Jiang; W. Wu; Y. He; H. Chung; and F. Blaabjerg, "New Passive Filter Design Method for Overvoltage Suppression and Bearing Currents Mitigation in a Long Cable Based PWM Inverter-Fed Motor Drive System," *IEEE Trans. on Power Electronics*, Vol. 32, Issue 10, pp. 7882-7893, 2017.

[3] O. S. Ebrahim, K. O. Shawky, M. A. Badr, P. K. Jain, "An Induction Motor Drive System with Intelligent Supervisory Control for Water Networks Including Storage Tank," *World Academy of Science, Engineering and Technology Inter. Journal of Mechanical and Industrial Eng.,*, Vol. 17, No. 3, 2023.

[4] I. Kioskesidis and N. Margaris, "Loss minimization in scalar controlled induction motor drives with search controller," *IEEE Trans. Power Electron.*, vol. 11, no. 2, pp. 213-220, 1996.

[5] B. K. Bose, N. R. Patel, and K. Rajashekara, "A neuro-fuzzy-based on-line efficiency optimization control of a stator flux-oriented direct vector-controlled induction motor drive," *IEEE Trans. Ind. Electron.*, vol. 44, no. 2, pp. 270-273, Apr. 1997.

[6] M. N. Uddin and S. W. Nam, "New online loss minimization-based control of an induction motor drive," *IEEE Trans. Power Electron.,* vol. 23, no. 2, pp. 926-033, Mar. 2008.

[7] H. Rasmussen, P. Vadstrup, and H. Borsting, "Rotor field oriented control with adaptive iron loss compensation," *in Proc. IEEE IAS Ann. Meeting*, vol. 2, pp. 1253–1258, Oct. 1999.

[8] F. Fernandez-Bernal, A. Garcia-Cerrada, and R. Faure, "Model based loss minimization for DC and AC vector-controlled motors including core saturation," *IEEE Trans. Ind. Appl.*, vol. 36, no. 3, pp. 755–763, May/Jun. 2000.

[9] C. Chakraborty and Y. Hori, "Fast efficiency optimization techniques for the indirect vector-controlled induction motor drives," *IEEE Trans. Ind. Appl.*, vol. 39, no. 4, pp. 1070–1076, Jul./Aug. 2003.

[10] S. K. Sul and M. H. Park, "A novel technique for optimal efficiency control of a current-source inverter-fed induction motor," *IEEE Trans. Power Electron.*, vol. 3, no. *2,* pp. 192-199, Apr. 1988.

[11] I. Kioskeridis and N. Margaris, "Loss minimization induction motor adjustable-speed drives," *IEEE Trans. Ind. Elec.*, vol. 43, no. 1, pp. 226-231, Feb. 1996.

[12] F. Abrahamsen, F. Blaabjerg, J. K. Pedersen, and P. B. Thoegersen, "Efficiency-optimized control of medium-size induction motor drives," *IEEE Trans. Ind. Appl.*, vol. 37, no. 6, pp. 1761–1767, Nov./Dec. 2001.

[13] T. W. Jian, N. L. Schmitz, and D. W. Novotny, "Characteristic induction motor slip values for variable voltage part load performance optimization," *IEEE Trans. Power App. Sysr.,* vol. PAS-102, no. 1, pp. 38-46, Jan. 1984.

[14] C. A. Hernandez-Aramburo, T. C. Green, and S. Smith, "Assessment of power losses of an inverter-driven induction machine with its experimental validation," *IEEE Trans. Ind. Appl.*, vol. 39, no. 4, pp. 994-1004, July/Aug. 2003.

[15] A. Boglietti, P. Ferraris, M. Lazzari and F. Profumo, "Effects of different modulation index on the iron losses in soft magnetic materials supplied by PWM inverter," *IEEE Trans. Magn.,* vol. 29, no. 6, pp. 3234-3236, Nov. 1993.

[16] A. Boglietti, "PWM Inverter fed induction motor losses evaluation," *Electric Machines and Power Systems,* no. 22, pp. 439-449, 1994.

[17] O. S. Ebrahim, A. S. Elgendy, M. A. Badr, and P. K. Jain," ANN-Based Optimal Energy Control of Induction Motor in Pumping Applications," IEEE Trans. on Energy Conversion, no.3.1, Oct. 2010.

[18] H. M. Jabr and N. C. Kar, "Leakage flux saturation effects on the transient performance of wound-rotor induction motors," *Elsevier Electr. Power Sys. Research*, vol. 78, no. 7, 1280–1289, 2008.

[19] R. Kaczmarek, M. Amar, and F. Protat, "Iron loss under PWM voltage supply on Epstein frame and in induction motor core," *IEEE Trans. Magn.,* vol. 32, no. 1, pp. 189-194, Jun. 1996.

[20] M. G. Say, "Alternating Current Machines", *John Wiley & Sons, 5th edition, 1968.*

[21] H. Zhao; C. Liu; Y. Zhan; and G. Xu,' Loss and Starting Performance of Inverter-Fed Induction Motors Considering Semi-Closed Effect of Closed Slot,' 2019 Inter. Applied Computational Electromagnetics Society Symposium (ACES), 2019.

[22] Bin Chen,' Analysis of Effect of Winding Interleaving on Leakage Inductance and Winding Loss of High Frequency Transformers,' *Journal of Electrical Engineering & Technology*, vol. 14, pp.1211–1221, 2019.

[23] D. G. Holmes and T. A. Lipo, "Pulse width modulation of power converters: Principles and practice," *IEEE Press Series on Power Eng.*, John Wiley, 2003.

[24] J. A. Snyman, "Practical mathematical optimization: an introduction to basic optimization theory and classical and new gradient-based algorithms," Springer Publishing, 2005.

[25] Bimal K. Bose, "Neural network applications in power electronics and motor drives—An introduction and perspective," *IEEE Trans. Ind. Electron.*, vol. 54, no. 1, pp. 14-33, Feb. 2007.

[26] P. Vas, "Artificial intelligence-based electrical machines and drives: Application of fuzzy, neural, fuzzy neural, and genetic algorithm based techniques," *Oxford Science Publications*, Oxford university press, 1999.

[27] MathWorks Neural Network Toolbox User's Guide, 2001.

[28] J. R. Pottebaum, "Optimal characteristics of a variable-frequency centrifugal pump motor drive," *IEEE Trans. Ind. Appl.,* vol. IA-20, no. 1 ,

pp. 23-31, Jan./Feb. 1984.
[29] N. Mohan, T. M. Undeland, and W. P. Robbins, 'Power Electronics: Converters, Applications, and Design,' 3rd Ed., Wiley publisher, 2002.
[30] Hitachi L100 Series Inverter Manual, 2002.
[31] K. Smith and S. Jain, "The Necessity and Challenges of Modeling and Coordinating Microprocessor Based Thermal Overload Functions for Device protection," *The 70 Ann. Conf. On Protective Relay Engineers (CPRE), 2017.*
[32] J. Holtz, 'Sensorless control of induction motor drives,' Proc. of the IEEE, Vol. 90, Issue 8, 2002.

**Osama S. Ebrahim** received his BSc (Hons), MSc, and PhD degrees from Ain Shams University, Egypt, in 1993, 1998 and *2004* respectively. Since 2005, he has been Assistant Professor in the Electrical Power and Machines Department, Ain Shams University, and has served as a consultant engineer for the Electrical and Mechanical Research Institute, National Water Research Center, Egypt, where he provides scientific guidance in developing energy efficient and environmentally friendly variable speed pumping units. He has pursued research activities as a postdoctoral fellow at the Centre for Energy and Power Electronics Research (ePOWER), Queen's University, Canada, in 2006 and since 2008, with grant funding from the Ontario Ministry of Research and Innovation. Dr. Ebrahim is a member of IEEE and of the Egyptian Syndicate of Engineering. he was a Treasurer of the IEEE Kingston Section, Canada in l applications to power electronic converters, automatic voltage regulators, sensorless motor drives, wind alternators and solar PV systems. 2008. His research interests include modern control theories and their digital applications.

**Mohamad A. Badr** received the BSc (Hons.) degree from Cairo University, Egypt, MSc degree from Ain-Shams University, Egypt, MASc and PhD degrees from University of Saskatchewan, Canada in 1965, 1969, 1971, and 1974, respectively. He is a Professor in the Electrical Power and Machines Department, Ain-Shams University since 1986. Currently, he is a chairman in the Egyptian Supreme Council for promoting faculty staff members to higher ranks and Dean of Faculty of Engineering and Technology, Future University, Egypt.

Dr. Badr has a considerable contribution in developing the electrical and environmental engineering in Egypt and Saudi Arabia where he directed many conferences, workshops, consultant units and held various teaching positions. Dr. Badr is awarded the Egyptian State Encouraging Award in Engineering Sciences in 1997 and nominated for the UNESCO science prize for outstanding contribution to the scientific development of a member state or region. He is also obtained the Egyptian State Award for Scientific Superiority in Engineering Sciences in 2004. His domain of research activities in the electrical power and machine applications includes interdisciplinary varieties and he published more than 100 conference and Journal papers and three scientific books.

**A. S. Elgendy**, received his BSc and Msc degrees in Electrical Power and Machines from Ain Shams University, Egypt in 2001 and 2008, respectively. During the period 2003 to 2008, he engaged the Mechanical and Electrical Research Institute of National Water Research Center, Egypt as a researcher Engineer where he participated in the commissioning and routine tests of large scale pumping stations and development of SCADA monitoring systems. Since June 2008 he joined IMPRESUB International Diving and Marin Contractors for offshore petroleum services as a Hydrographic Survey Engineer. Mr. Elgendy is a member of the Egyptian Syndicate of Engineering. His research interests includes efficiency optimization of electric machines, variable speed drives utility interface and control, and analysis of hydrographic data.

**Kareem O. Shawky** is a student at the Civil Dept., Faculty of Engineering, Ain Shams University, Egypt. His research interest includes smart cities, building and hydro storage systems and networks, traffic management and control and intelligent cloud computing.

**Praveen K. Jain** (S'86, M'88, SM'91, F'02) received a BE (Hons.) degree from the University of Allahabad, India, and MASc and PhD degrees from the University of Toronto, Canada, in 1980, 1984, and 1987, respectively, all in electrical engineering.

Presently, he is a Professor and Tier-1 Canada Research Chair in Power Electronics at Queen's University in Kingston, Ontario, Canada. He is also the founding Director of the Queen's Centre for Energy and Power Electronics Research (ePOWER).

From 1994 to 2000, Dr. Jain was a Professor at Concordia University, Montreal, Canada, where was engaged in teaching and research in the field of power electronics. Prior to this (1989-1994) he was a Technical Advisor with the Power Group, Nortel Networks, Ottawa, Canada, where he was providing guidance for research and development of advanced power technologies for telecommunications. During 1987-1989, he was with Canadian Astronautics Ltd., Ottawa, Canada, where he played a key role in the design and development of high frequency power conversion equipments for the Space Station Freedom. He was a design engineer and production engineer at Brown Boveri Company and Crompton Greaves Ltd., India, respectively during the period of 1980-1981. He also has considerable consulting experience with the industry including Astec, Ballard, General Electric, Intel and Nortel.

Dr. Jain has attracted over $20M funding to conduct research and establish the state-of-the-art Energy and Power Electronics Applied Research Laboratory (ePEARL) at Queen's University. He has also supervised over 75 research engineers, postdoctoral fellows and graduate students. He has considerable experience in transferring technology from university lab to practical product designs. He secured over $35M venture funding to found CHiL Semiconductor to design and market mixed analog/digital semiconductor chip products. Dr. Jain has published over 375 publications including 40 patents in the area of power electronics. Dr. Jain is a Fellow of the Institute of Electrical and Electronics Engineering (FIEEE), a Fellow of the Engineering Institute of Canada (FEIC) and a Fellow of the Canadian Academy of Engineering (FCAE). He is also the recipient of 2004 Engineering Medal (R&D) of the Professional Engineers of Ontario. He is an Associate Editor of IEEE Transactions on Power Electronics, and KIPE Journal of Power Electronics. Recently, Dr. Jain has been awarded the 2021 IEEE Medal in Power Engineering.